Supporting Information

Manneville *et al*. 10.1073/pnas.0807102105

SI Materials and Methods

Labeling of Arf1 with Oregon Green Maleimide. An extra C-terminal cysteine (C182) was added by PCR to the sequence of bovine Arf1 cloned into a pET11d vector (Novagen). [C182]Arf1 was coexpressed in *E Coli* with N-myristoyl transferase in the presence of myristate/BSA. The myristoylated form, which is bound to GDP, was purified from the soluble fraction by ammonium sulfate precipitation followed by DEAE and MonoS chromatography under reducing conditions (e.g., in the presence of 1 mM DTT) as described for the wild-type form (1). The protein was stored at −80 °C.

Before labeling, the protein buffer was replaced by a freshly degassed buffer containing no DTT (20 mM Hepes, pH 7.5, 100 mM NaCl, and 1 mM $MgCl_2$) using an NAP-10 column. A stock solution of Oregon Green 488 maleimide (Molecular Probes) was prepared in dimethylformamide (DMF). Labeling was performed at room temperature with 10 μM [C182]Arf1-GDP, 100 μM GDP, and 100 μM Oregon Green 488 maleimide (the final concentration of DMF was <0.5%). After one min, the reaction was stopped by the addition of 10 mM DTT and the sample was applied to a NAP-10 column to separate protein from excess probe. Aliquots before and after the reaction were analyzed by SDS/PAGE. The protein gel (13% acrylamide) was first visualized directly in a fluorescence imaging system (FUJI LAS 3000) to identify labeled proteins. Then the gel was stained with Sypro-Orange to visualize all proteins. A shift in the mobility of Arf1 permits to detect the labeled form (Arf1-OG) from the unlabelled one. Labeling was complete within the first minute of incubation. It should be noted that wild-type Arf1 contains a single cysteine at position 159, which is buried in the nucleotide-binding pocket. Control experiments with this form showed no detectable labeling with Oregon-green after 10-min incubation. This suggests that the extra cysteine introduced at position 182 of Arf1 is the sole residue that is labeled by Oregon green maleimide.

Labeling of Coatomer with Tetramethyl Rhodamine. Coatomer was purified from rabbit liver as described in ref. 2 except that we included a gel-filtration step (Sephacryl S-300) before the last source Q chromatography. A stock solution of tetramethyl rhodamine (TMR)-maleimide (Molecular Probes) was prepared in DMSO. Before labeling, coatomer (500 μl, 3 μM) was applied to a NAP-5 column and eluted with a freshly degassed buffer containing no DTT (50 mM Hepes, pH 7.2, 120 mM potassium acetate, and 1 mM $MgCl_2$). The protein pool was then incubated with a 10 molar excess of TMR-maleimide for 30 min at 4 °C (the final concentration of DMSO was <0.01%). The reaction was stopped by the addition of 10 mM DTT and the sample was applied to a NAP-5 column equilibrated with HKM buffer containing 10% glycerol to separate proteins from excess probe. The protein pool was centrifuged at 45,000 rpm in a TLA100 rotor for 10 min to eliminate aggregates and stored at −80 °C. Aliquots before and after the reaction were analyzed by SDS/PAGE. The protein gel (8% acrylamide) was first visualized in a fluorescence imaging system (ProXPRESS, Perkin–Elmer) upon excitation at 550 nm and emission at 590 nm to identify labeled proteins. Then the gel was stained with Sypro-orange to visualize all proteins.

FRAP Experiments on Arf1-OG. FRAP was performed on a LSM510 Zeiss confocal microscope using the Argon 488-nm laser line. The image was focused at the bottom of the GUVs on the membrane close to the coverslip. A 32 × 32 pixels zone was imaged at 20–25 frames/s. A prebleach series of 500 frames were taken at low laser power (0.1–0.5% total power) to avoid photobleaching. Arf1-OG fluorescence was bleached in a circular region (10 to 30 pixels in diameter corresponding to radii R_{bleach} from 1.5 to 6.8 μm) for 0.2 s at maximal laser power. Fluorescence recovery was measured in the circular region during 750–1,500 frames. The half-time for recovery $\tau_{1/2}$ was obtained by fitting the recovery curves $F(t)$ using: $F(t) = (F_{post} + F_{recovery}\ t/\tau_{1/2})/(1 + t/\tau_{1/2})$, where F_{post} and $F_{recovery}$ are fit parameters for the fluorescence intensity just after bleaching and after recovery respectively (3). The mobile fraction R was calculated according to: $R = (F_{recovery} - F_{post})/(F_{pre} - F_{post})$, where F_{pre} is the prebleach fluorescence intensity averaged over the 500 frames prebleach series. The diffusion coefficient was obtained using $D = R_{bleach}^2/4\tau_{1/2}$ (see Table S1). Because the area of the bleached region is negligible compared with the total GUV membrane area, the maximal recovery is $R \approx 100\%$.

FRAP Experiments to Compare Coatomer-TMR Mobility with the Mobility of Arf1-OG and Fluorescent Lipids. FRAP was performed on a Nikon Eclipse C1si confocal microscope. The image was focused in the equatorial plane of the GUV on a zone containing coatomer-TMR signal from weakly curved domains. A 160 × 160 pixels zone was imaged at 3–4 frames/s. A prebleach series of 10 frames (3.5 s) were taken at low laser power (0.1–0.5% total power) to avoid photobleaching. Coatomer-TMR fluorescence was bleached in a rectangular region covering ≈ 20 to 30% of the GUV surface at maximal laser power (561 nm). Fluorescence recovery was measured in the circular region during 100 frames (35 s). The averaged recovery curve (n = 27–31 GUVs) was fitted using the same equations as above to yield the half-time for recovery $\tau_{1/2}$ and the mobile fraction R (see Table S2). The recovery of coatomer-TMR was compared with that of free Arf1-OG (bleached at 488 nm) and fluorescent lipids, as measured in the same geometry of photobleaching. In the case of fluorescent lipids, data from three different types of lipids were pooled (Ceramide-BodipyTR and DHPE-TexasRed bleached at 561 nm; C5-HPC-BodipyFL bleached at 488 nm). Because a significant fraction (20–30%) of the fluorophores is irreversibly photobleached, the maximal recovery is $R \approx 75\%$.

Visualization of Coatomer Bound to GUVs Using a Fluorescently Labeled anti-β-COP Antibody. The Zenon protocol (Z25002 from Molecular Probes) was used to couple the green fluorescent dye Alexa488 to an anti-β-COP antibody (clone maD G6160 from Sigma). Vesicles containing 1% Ceramide-BodipyTR (Invitrogen) were incubated for 20 min in the presence of 0.5 μM Arf1 and 0.15 μM coatomer in HKM buffer, 2 mM EDTA, and 0.1 mM GTPγS. One microliter of fluorescently labeled antibody was added to the vesicles. After 10-min incubation at 37 °C, the vesicles were transferred to and observed in a chamber as described in Materials and Methods.

Fluorescence Quantification. The amount of fluorescent protein bound to GUV membranes F_{ves} was quantified by measuring the average fluorescence of the membrane using the OvalProfile macro in the ImageJ software. The background fluorescence due to unbound protein F_{back} was measured in an area close to the vesicle. The vesicle fluorescence intensity was defined as $I = (F_{ves} - F_{back})/F_{back}$. When different experimental conditions were compared, images of protein fluorescence were taken with

the same illumination and detection settings. Results are given ± SEM.

Quantification of Membrane Deformation. To assess the morphology of membrane bound coatomer on GUVs, we classified vesicles into four categories: (1) spherical GUVs completely covered with coatomer-TMR or exhibiting large (> 1 μm and up to 5 μm) static quasi-flat domains (designed as 'large domains'), (2) spherical GUVs showing small (< 1 μm) dynamic and weakly curved patches (designed as 'patches'), (3) deformed GUVs with small dynamic budded profiles ('small profiles') and (4) deformed GUVs with dynamic tubular profiles ('large profiles'). In the case of vesicles exhibiting deformations, the total number of small profiles (N_s) or large profiles (N_l) was counted from 3D confocal scans of the GUVs. The percentage of GUVs from each category was scored.

We used the ImageJ software to measure the circularity of the GUVs from confocal images taken in the GUV equatorial plane, in the presence or absence of 10 μg/ml SLO and in the presence or absence of coatomer-TMR. The circularity is defined as the ratio $4\pi\ Area_{ves}/(Perim_{ves})^2$, where $Area_{ves}$ and $Perim_{ves}$ are the vesicle area and perimeter respectively, and equals one for a circle. To quantify more precisely the deformation of the membrane, we measured the membrane length enclosed in the deformations (corresponding to the projected area of membrane deformations) from confocal sections in the equatorial plane. We defined a deformation index as $(Perim_{ves} - Perim_{fit})/Perim_{fit}$, where $Perim_{ves}$ is the perimeter of the vesicle external contour measured in the equatorial plane (including deformation profiles), and $Perim_{fit}$ is the perimeter of the best ellipse fit of the inside contour of the vesicle (excluding deformation profiles). The deformation index equals zero for an elliptical vesicle. Statistical significance was assessed using Student's t test.

Electron Microscopy of COPI-coated GUVs. Electroformed Golgi mix GUVs were first concentrated 20 times by centrifugation (210 rcf, 30 min, room temperature) in osmotically balanced buffer in a bacitracin (10 mg/ml) coated 0.5 ml Eppendorf tube. Two microliters of GUVs were incubated with Arf1, coatomer, and SLO in the same conditions as described above. COP-I coated GUVs were transferred to a PolyL-lysin (0.1%) coated Beem embedding capsule (ref. 70000-B Electron Microscopy Sciences) and centrifuged at room temperature for 15 min at 4,000 rpm in a swinging rotor (Jouan, GR412). The presence of a GUV pellet was checked by epifluorescence through the bottom of the Beem capsule. The sample was fixed with 2.5% glutaraldehyde in phosphate buffer, postfixed with 1% osmium tetroxide in cacodylate buffer, dehydrated in a series of alcohol, embedded in epoxy resin and processed for EM observation. The sections were observed in a Philips CM12 electron microscope operating at 80 kV and pictures were taken on Kodak electron microscope films 4489.

1. Franco M, *et al.* (1995) Myristoylation of ADP-ribosylation factor 1 facilitates nucleotide exchange at physiological Mg_{2+} levels. *J Biol Chem* 270:1337–1341.
2. Nickel W, Wieland FT (2001) Receptor-dependent formation of COPI-coated vesicles from chemically defined donor liposomes. *Methods Enzymol* 329:388–401.
3. Yguerabide, *et al.* (1982) Lateral mobility in membranes as detected by fluorescence recovery after photobleaching. *Biophys J* 40:69–75.
4. Bigay J, *et al.* (2005) ArfGAP1 responds to membrane curvature through the folding of a lipid packing sensor motif. *EMBO J* 24:2244–53.

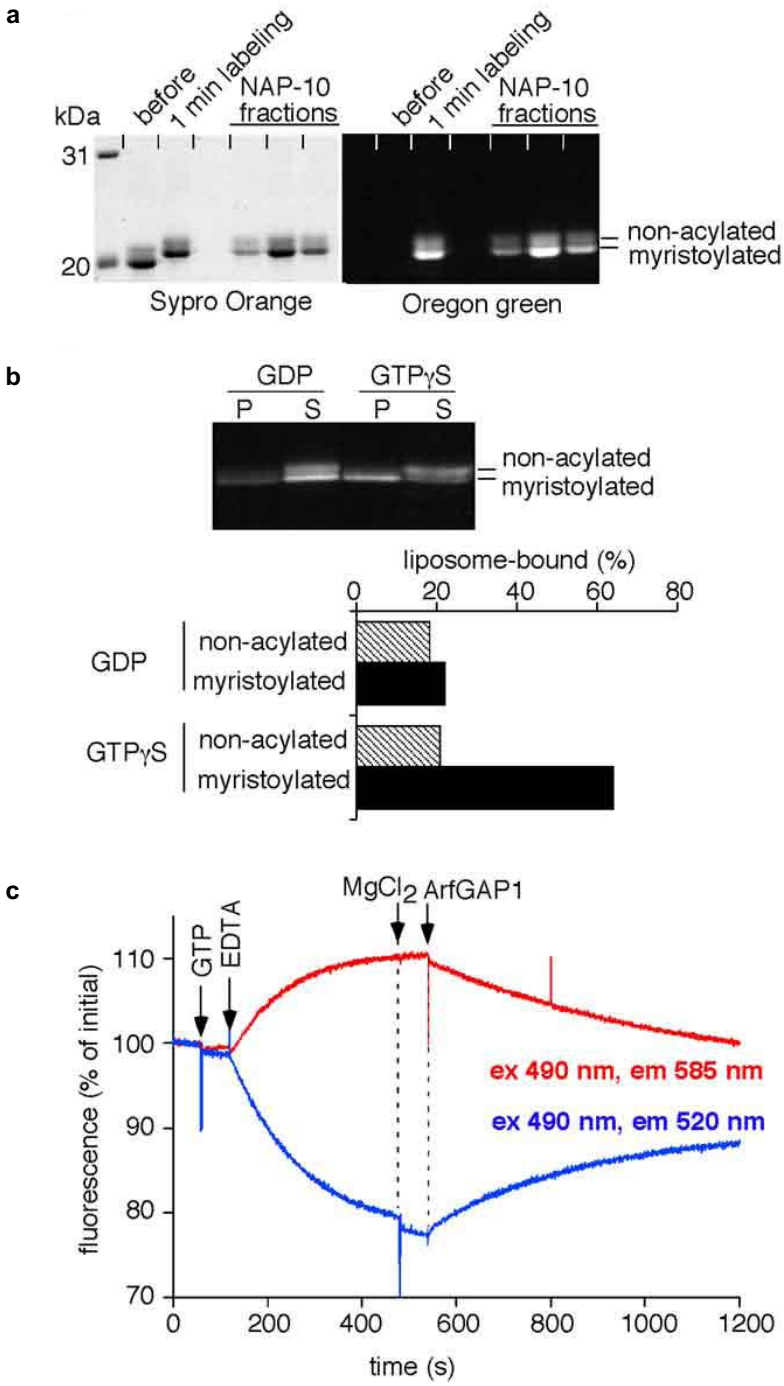

Fig. S1. Preparation and characterization of Arf1-OG. (*A*) SDS/PAGE analysis of [C182]Arf1-GDP before and after labeling with Oregon-Green (OG) maleimide for 1 min. Fractions from the NAP-10 column, which was used to remove excess probe, are also shown. The gel was directly visualized in a fluorescence imaging system to detect labeled proteins (*Right*) and then stained with sypro-orange to visualize all proteins (*Left*). Note that labeling reduces the mobility of Arf1. (*B*) Liposome binding experiment. Arf1-OG-GDP was incubated at 37 °C with sucrose-loaded Golgi-mix liposomes (0.3 mM, obtained by extrusion through a 0.4-μm polycarbonate filter) in the presence of GDP or GTPγS (100 μM) and under conditions that promote nucleotide exchange (HKM buffer supplemented with 2 mM EDTA giving 1 μM free Mg^{2+}). After 15 min, 2 mM $MgCl_2$ was added to stop nucleotide exchange and the sample was centrifuged at 400,000 $\times$ *g* for 15 min at 4 °C in a TL100 rotor. The supernatant and the lipid pellet were analyzed by SDS/PAGE. Note that only the myristoylated form of Arf1-OG binds in a GTP-dependent manner to the liposome. (*C*) The GTP-dependent translocation of Arf1-OG to liposomes could be also observed by Fluorescence Resonance Energy Transfer (FRET) using liposomes containing Rhodamine-phosphatidylethanolamine (PE). One micromolar Arf1-OG-GDP was mixed with 0.3 mM Golgi-mix liposomes containing 1% rhodamine-PE in HKM buffer. At the time indicated GTP (100 μM) and EDTA (2 mM, giving 1 μM free Mg^{2+}) were added to promote nucleotide exchange. FRET was measured either at 585 nm (acceptor fluorescence) or at 520 nm (donor fluorescence) upon excitation at 490 nm. After nucleotide exchange, 2 mM $MgCl_2$ was added followed by the addition of 50 nM ArfGAP1, which hydrolyses GTP in Arf1 and thus reverses the fluorescence signal.

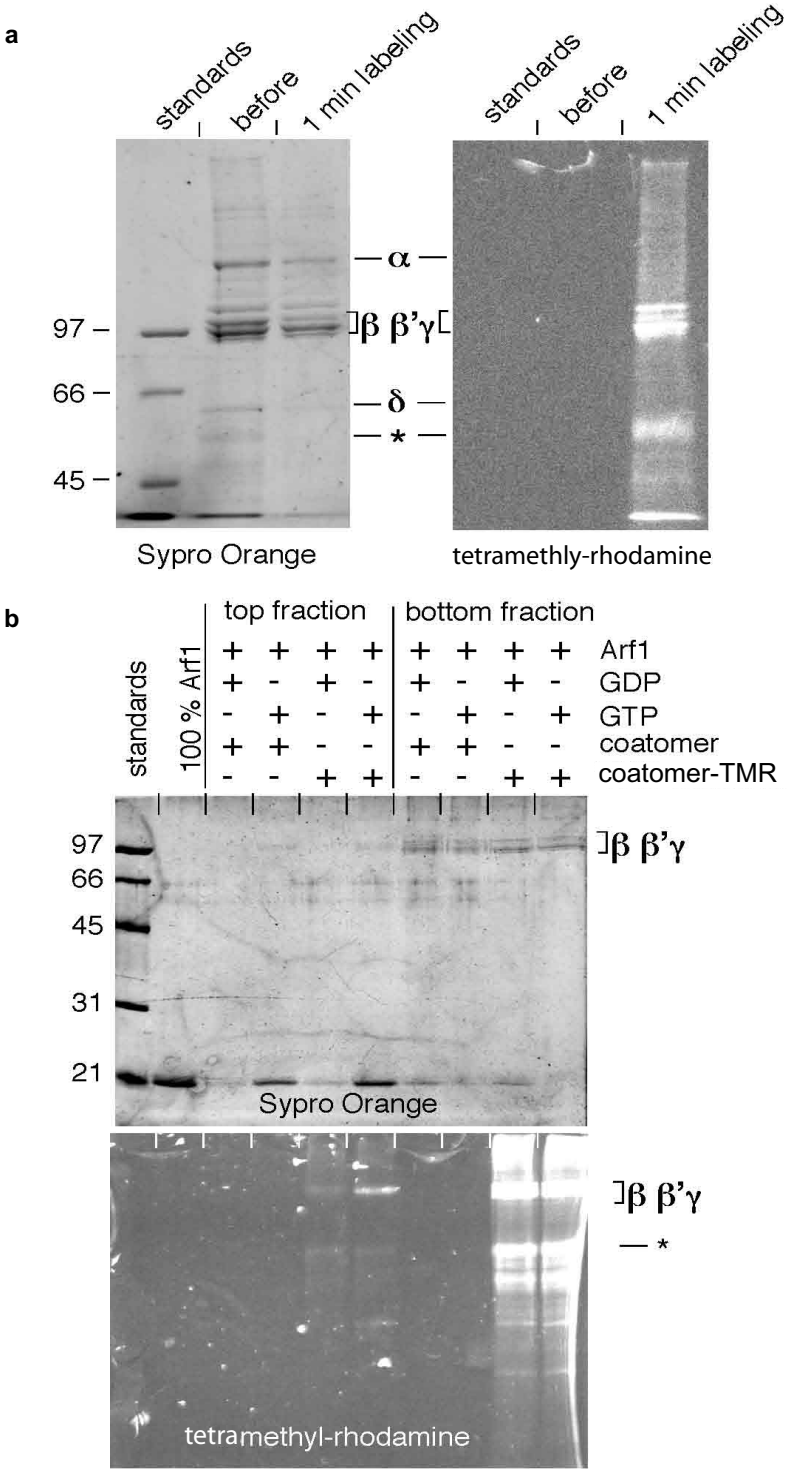

Fig. S2. Preparation and characterization of coatomer-TMR. (*A*) SDS/PAGE analysis of coatomer purified from rabbit liver before and after labeling with tetramethyl-rhodamine (TMR) maleimide for 30 min at 4 °C. The gel was first visualized in a ProXpress imaging system (excitation 550 nm emission 590 nm) to detect TMR-labeled proteins (*Right*) and then stained with sypro-orange to visualize all proteins (left). Note that most labeling was observed on the 100-kDa subunits (β, β', γ) of coatomer. However, a contaminant at ≈50 kDa was also labeled (*). (*B*) Flotation experiment. Arf1-GDP (1 μM) was incubated with coatomer or with TMR-labeled coatomer (0.15 μM) in the presence of Golgi mix liposomes (0.3 mM) supplemented with the Lp23 lipopeptide and with GDP or GTP in HKM buffer supplemented with 2 mM EDTA. After 5 min at 37 °C, liposome bound proteins were recovered by centrifugation at the top of sucrose cushions (top fractions) whereas unbound proteins were recovered in the bottom fraction (4). The fractions were analyzed by SDS/PAGE and the gel was visualized either in a ProXpress imaging system (excitation 550 nm emission 590 nm) to detect TMR-labeled proteins or after sypro-orange staining to detect all proteins.

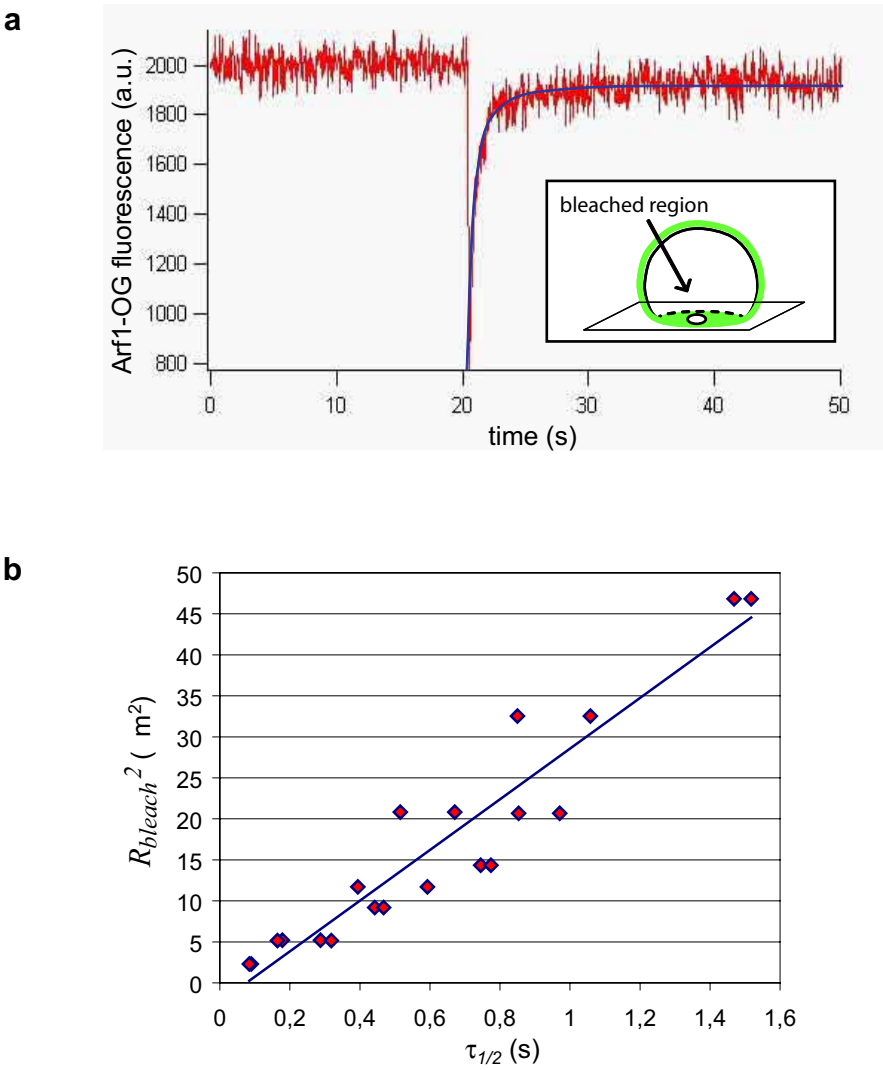

Fig. S3. Mobility of Arf1 on model membranes. (*A*) Typical FRAP curve showing recovery of Arf1-OG fluorescence after photobleaching (red line). Bleaching occurs after a 20 s (500 frames) prebleach observation period. The blue line shows the fit to the data yielding the half-time for recovery and the mobile fraction (see *SI Materials and Methods*). Since the photobleached region (small circular area at the bottom membrane of the GUV, see *Inset*) is negligible compared with the total GUV area, the maximal recovery is ≈100%. (*B*) The bleach area R^2_{bleach} varies linearly with the half-time for recovery $\tau_{1/2}$ showing that Arf1 mobility is dominated by 2D free diffusion.

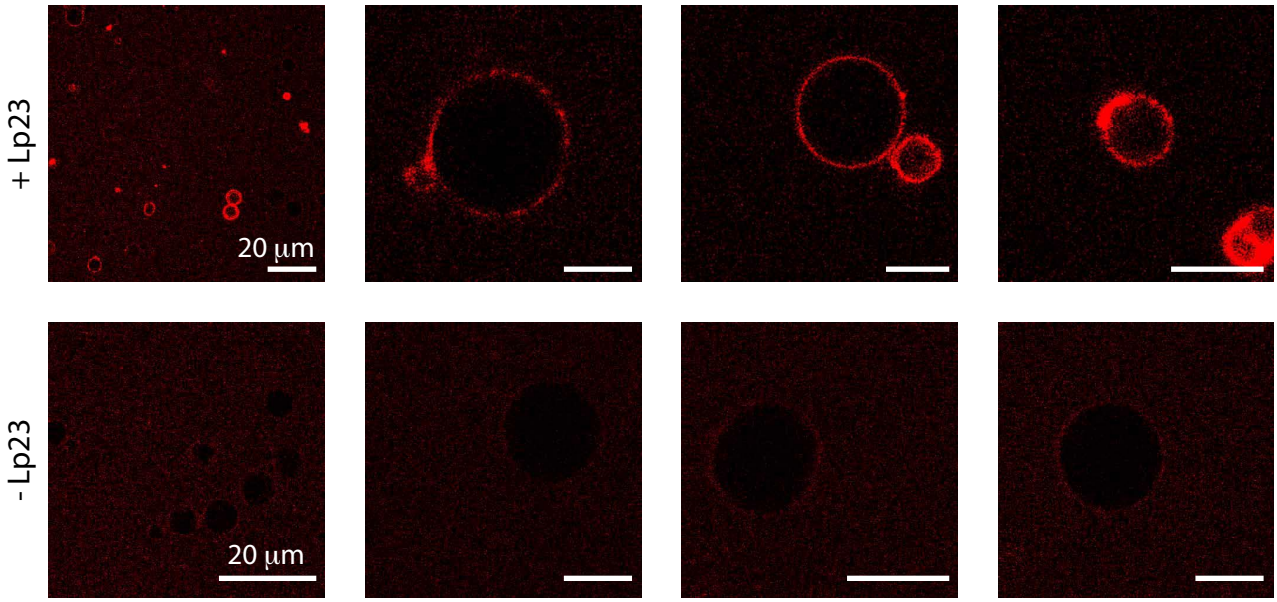

Fig. S4. The lipopeptide Lp23 increases coatomer binding to GUV membranes. Comparison of coatomer-TMR binding in the presence (upper row, +Lp23) or in the absence (lower row, −Lp23) of 1.5% (mol/mol) Lp23. The experimental conditions are the same as in Fig. 1*B*. Red: coatomer-TMR. (Scale bars, 5 μm or as indicated.)

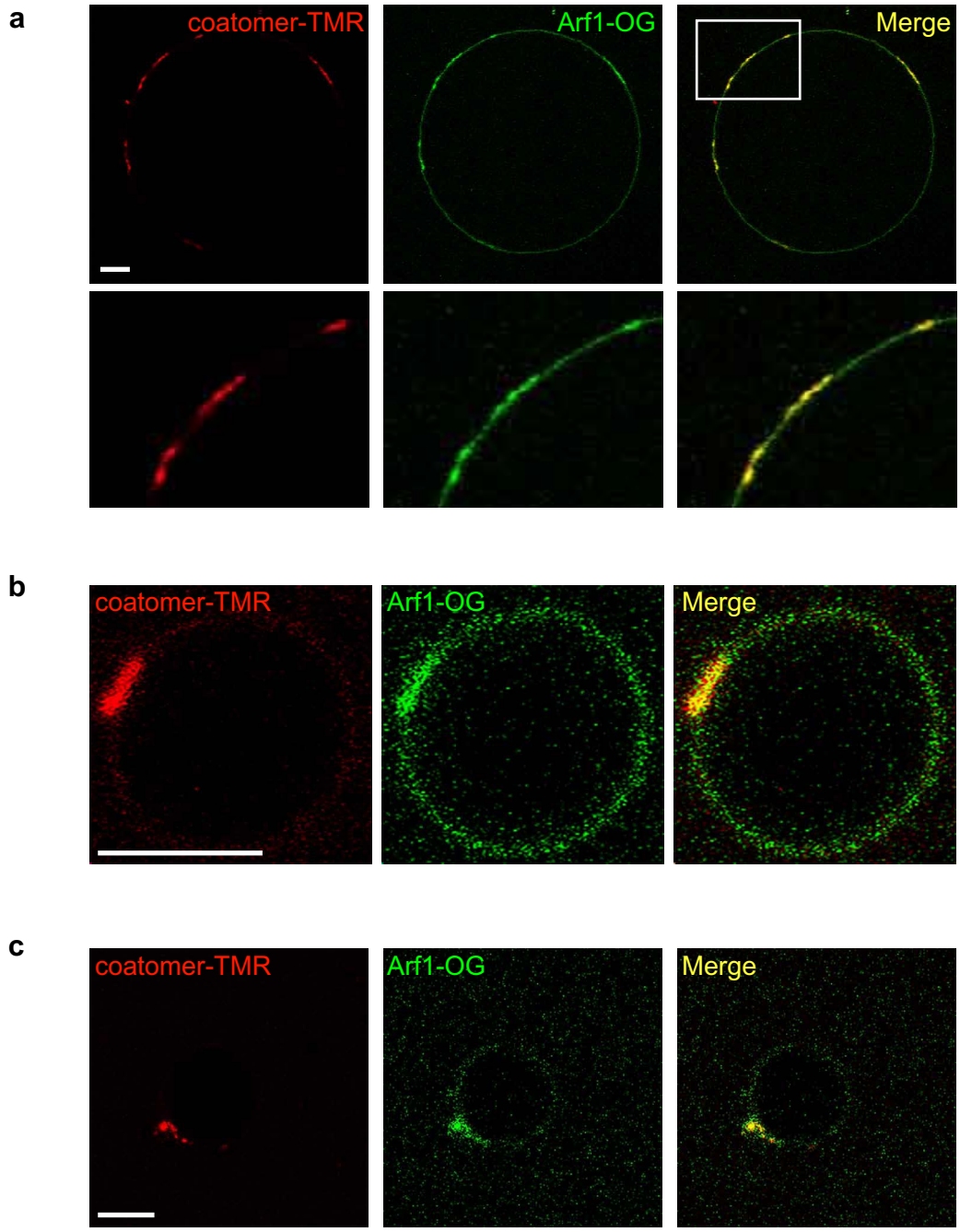

Fig. S5. Arf1 is enriched in coatomer domains. Coatomer-TMR (red, left images) was incubated in the presence of Arf1-OG (green, *Middle* images) and GTP. (*A*) and (*B*) Weakly curved coatomer domains enriched in Arf1-OG (*Lower* in *A* show a magnified view of the boxed region). (*C*) Coatomer-induced deformation. (Scale bars, 5 μm.)

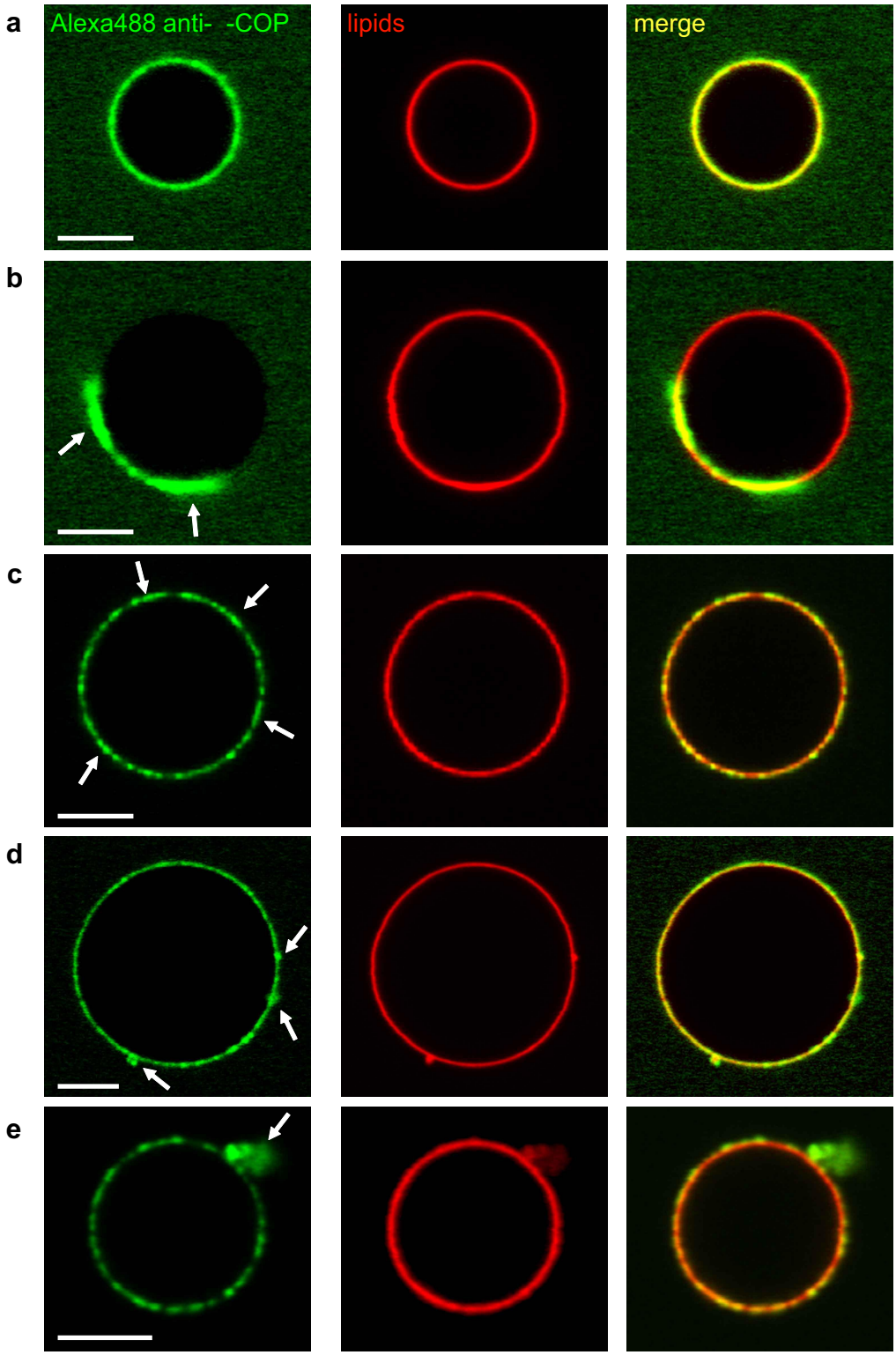

Fig. S6. Visualization of coatomer bound to GUVs using a fluorescently labeled antibody. The same membrane bound coatomer structures are observed as with coatomer-TMR: (*A*) GUVs completely covered with coatomer, (*B*) extended weakly curved domains, (*C*) small dynamic patches diffusing in the membrane plane, (*D*) dynamic budded profiles, and (*E*) tubular deformation profiles. Arrows in (*B–E*) point to coatomer-positive structures. Coatomer (green, *Left* images) is labeled by an anti-β-COP antibody coupled to Alexa488 (see *SI Materials and Methods*). Lipids (red, middle images) are shown by 1% Ceramide-BodipyTR. The merged images are shown on the *Right* images. (Scale bars, 5 μm.)

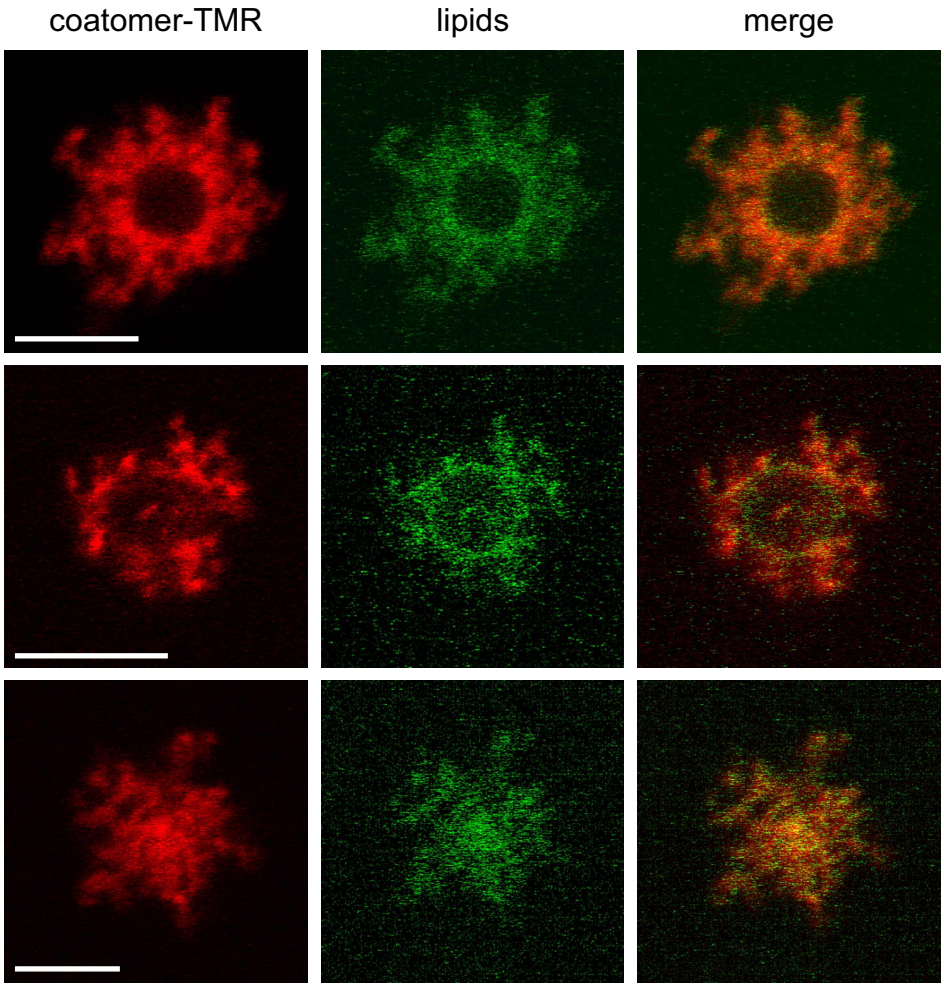

Fig. S7. Coatomer binding on low tension GUVs can induce extensive membrane deformation, vesicle shrinking and collapse. Three examples are shown. (Scale bars, 5 μm.)

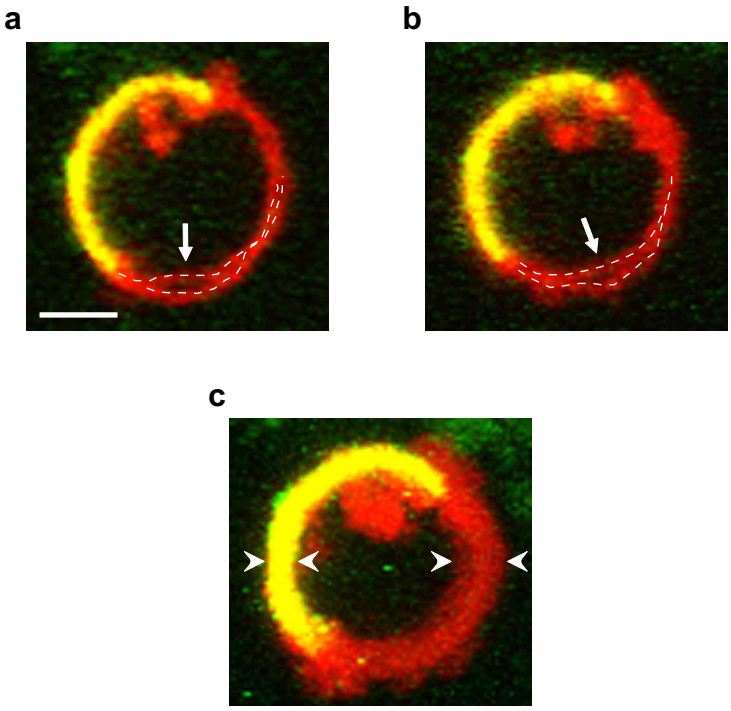

Fig. S8. Reducing membrane tension of an initially weakly curved coat does not lead to membrane deformation. Coatomer was first allowed to bind to a GUV under tension in the presence of Arf1 and GTP and to form a weakly curved domain. SLO was then added to reduce membrane tension. (*A*) and (*B*) Superimposition of two consecutive frames from Movie S13 showing that membrane fluctuations occur in the non-coated region of the GUV (dotted lines and white arrows). Two examples are shown at two different time points in the movie. Lipids are shown in red, and coatomer is detected using a green fluorescently labeled antibody (see Fig. S6). Yellow shows colocalization of red and green signals. (Scale bar, 2 μm). (*C*) 'Maximum' filter applied to Movie S13 showing the maximum value of the fluorescence intensity taken by each pixel throughout the movie. The amplitude of fluctuations (indicated between white arrowheads) is twice larger in the non-coated area (red, right side of the GUV) than in the coatomer-coated area (yellow, left side of the GUV). Quantification gives a maximum membrane displacement of 1.9 $\pm$ 0.2 μm in coatomer-free regions vs. 0.9 $\pm$ 0.1 μm in coatomer-coated regions (n = 10).

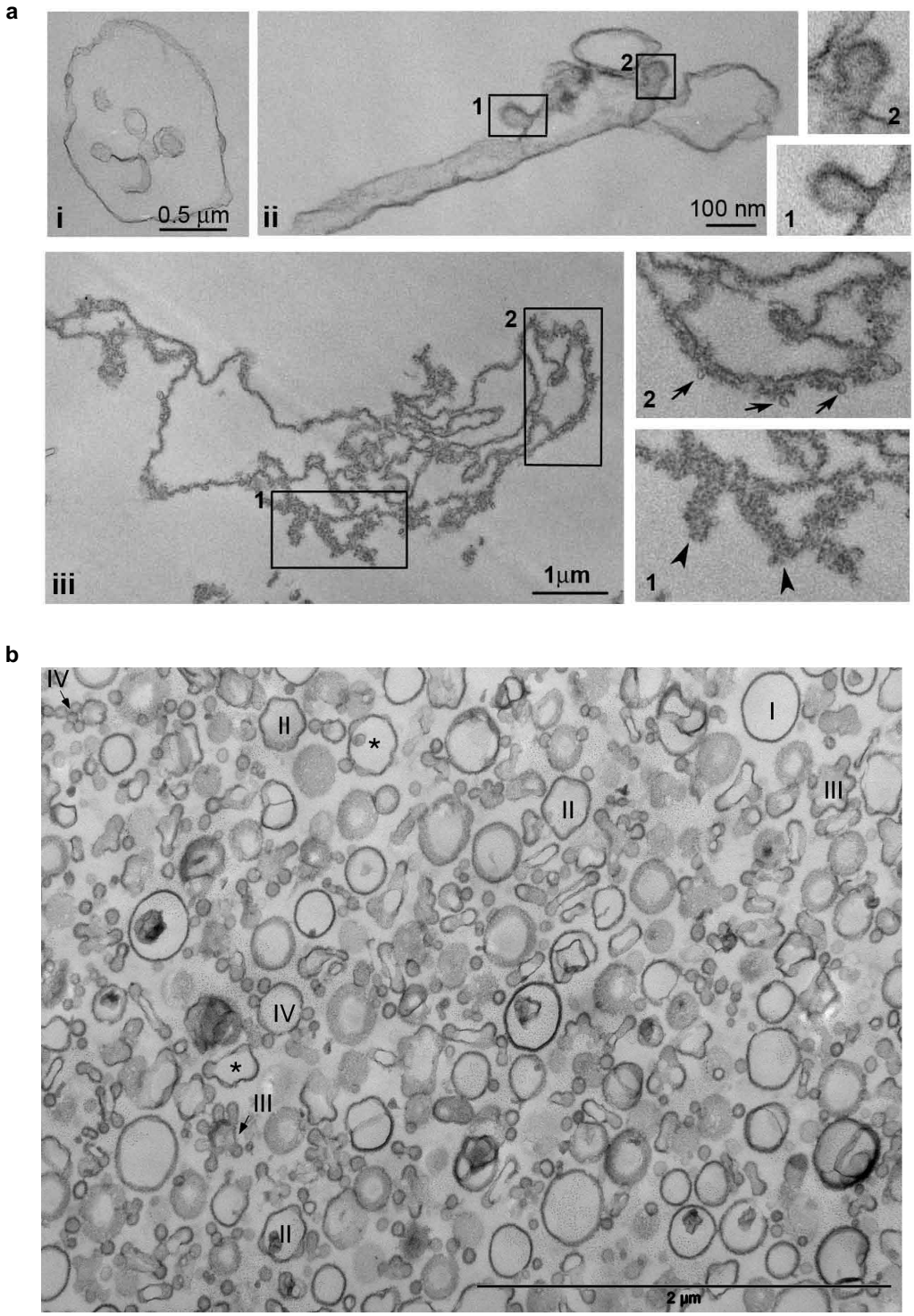

Fig. S9. COPI-induced deformations on GUVs and extruded liposomes. (*A*) Ultrastructural characterization of COPI-coated deformations on GUV membranes. GUVs were incubated with SLO, Arf1, GTP and coatomer-TMR in the same conditions as in light microscopy experiments. (i) Uncoated GUV. Bar, 500 nm. (ii) Typical COPI-coated buds on GUV membrane. The *Insets* show two 60-nm diameter coated buds. Bar, 100 nm. (iii) GUV membrane exhibiting extensively coated areas. Boxed regions show tubular profiles (arrowheads in *Inset* 1) and small 60-nm budded profiles (arrows in *Inset* 2). (Scale bar, 1 μm) *Insets* are enlarged 2$\times$ compared with the main panels. (*B*) This figure shows a low magnification view of the liposome pellet from which the COPI budding profiles shown in Fig. 3 were selected. Although the liposomes are clearly heterogeneous, there is a striking homogeneity in the shape of the budding profiles that emerge from the same liposome. Few examples are indicated: I, spherical liposomes; II, liposomes with several weakly curved buds; III, liposomes with intermediate budding profiles; IV, liposomes with complete budding profiles; * liposomes with non homogeneous budding profiles. (Scale bar, 2 μm.)

Movie S1. Mobility of Arf1-OG visualized by FRAP. Arf1-OG fluorescence is imaged at 20 frames/s in a 32 × 32 pixels (7 × 7 μm) region in the membrane of the GUV close to the coverslip. After 500 frames, fluorescence is bleached in a circular region (18 pixels in diameter) and recovery is monitored over another 1,000 frames.

Movie S1 (AVI)

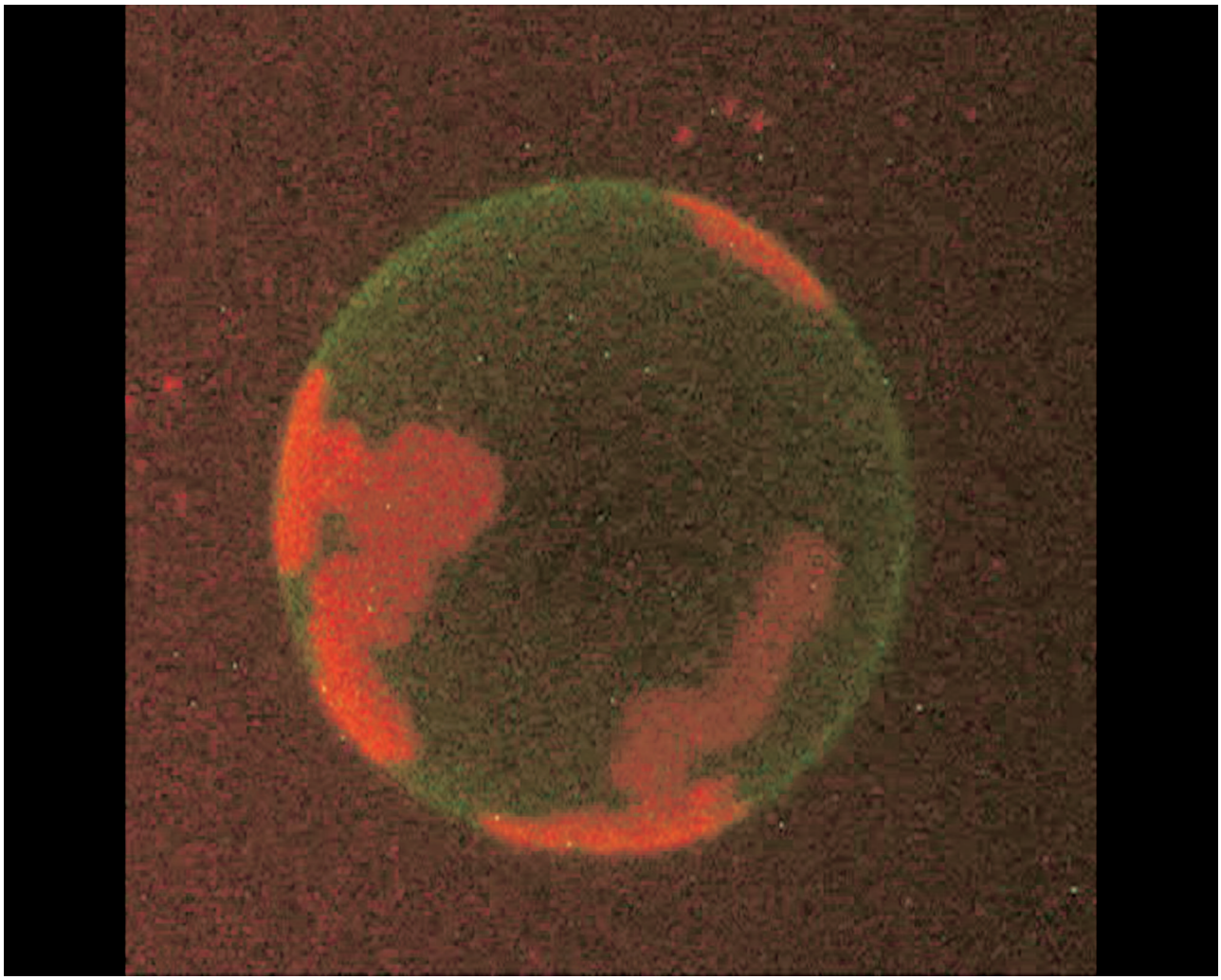

Movie S2. 3D reconstitution of coatomer bound to a tense vesicle. Coatomer-TMR (in red) forms extended domains on the surface of the vesicle (lipids are labeled by 0.5% C5-HPC-Bodipy-FL in green). These domains can be as large as 5–7 μm in diameter and have the same very weak curvature as the vesicle.

Movie S2 (MPG)

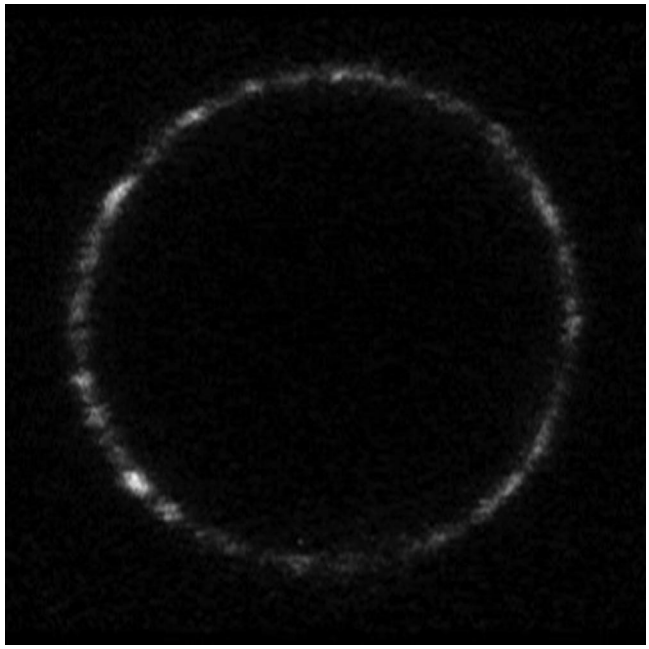

Movie S3. Dynamics of coatomer bound to a tense vesicle. Coatomer-TMR forms small dynamic patches that do not show any detectable curvature at the resolution of confocal microscopy. Note that the vesicle shape slightly deviates from a sphere.

Movie S3 (MPG)

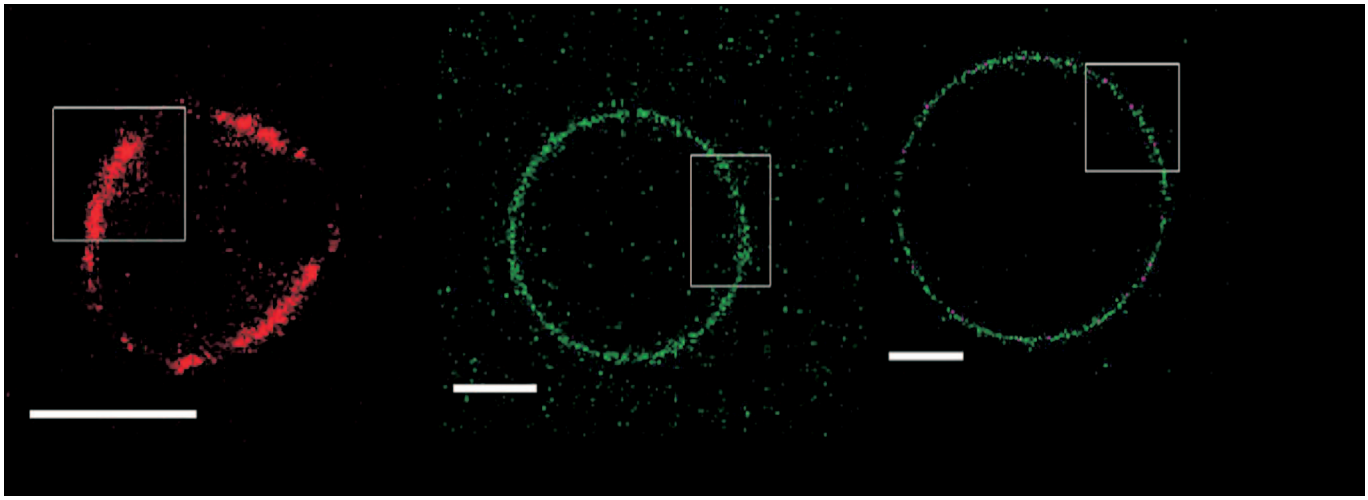

Movie S4. Mobility of coatomer-TMR compared with Arf1-OG and fluorescent lipids in FRAP experiments. Fluorescent signals from coatomer-TMR (*Left*), Arf1-OG (*Middle*) and the labeled lipid C5-HPC-BodipyFL (*Right*) are imaged in a confocal equatorial section of a GUV at 3 frames/s. After 10 frames, fluorescence is bleached in a rectangular region (white box) and recovery is monitored over another 100 frames. Coatomer-TMR fluorescence recovery is much slower than that of Arf1-OG and fluorescent lipids, and is due to diffusion of small-sized non-bleached patches from non-bleached regions into the bleached region.

Movie S4 (MPG)

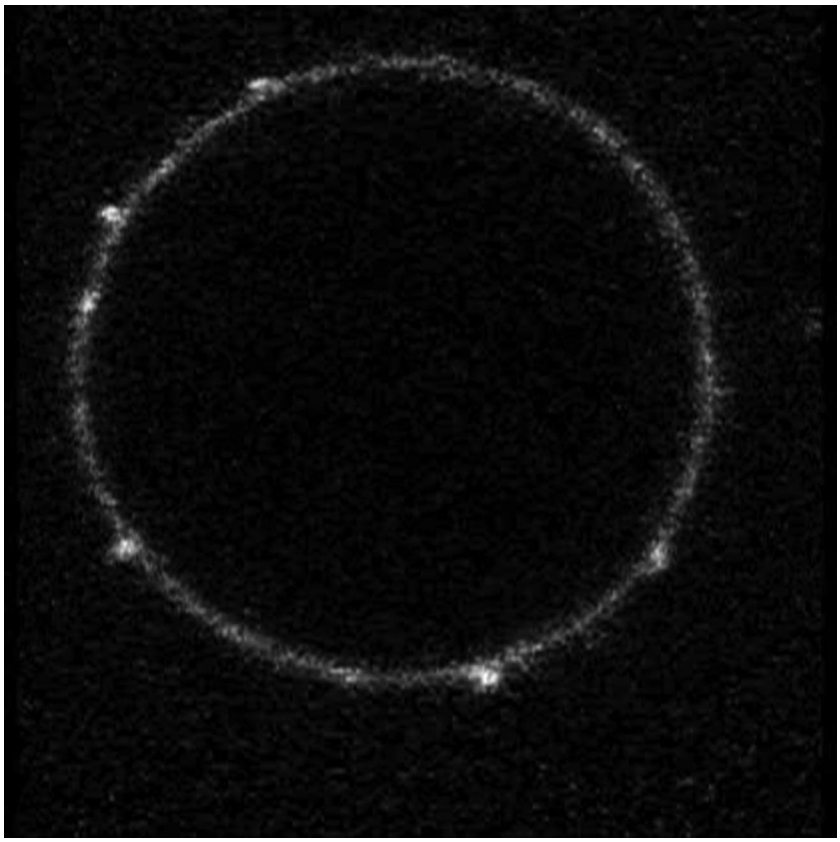

Movie S5. Dynamics of coatomer bound to a tense vesicle. Coatomer-TMR forms small dynamic deformation profiles enriched in coatomer-TMR that move in the plane of the membrane. The movie shows a confocal section in the equatorial plane of the vesicle. Note that the vesicle shape slightly deviates from a sphere.

Movie S5 (MPG)

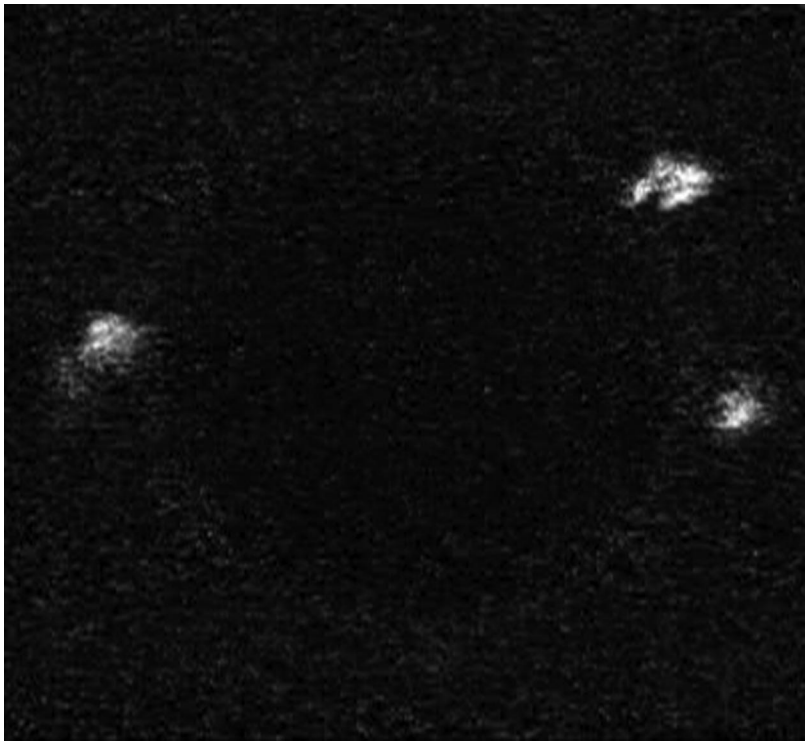

Movie S6. Dynamics of coatomer bound to a vesicle exhibiting weak membrane fluctuations. Large tubular profiles strongly enriched in coatomer-TMR are observed on the surface of the vesicle. Small membrane shape fluctuations indicate a lower membrane tension than in Movies S2–S5.

Movie S6 (MPG)

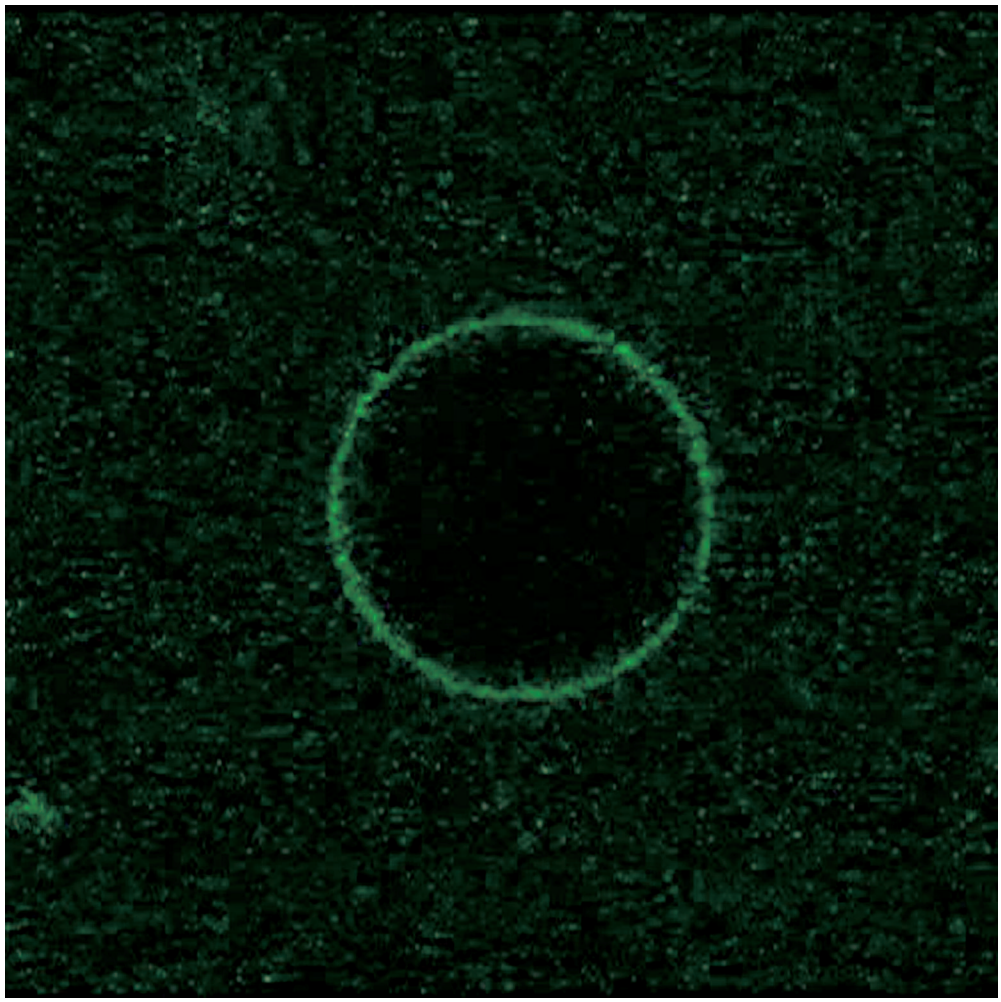

Movie S7. Movie S7 shows a control vesicle in the absence of SLO. The vesicles were incubated in the presence of 0.5 μM Arf1-OG (in green), 0.1 mM GTP, and 2 mM EDTA.

Movie S7 (MPG)

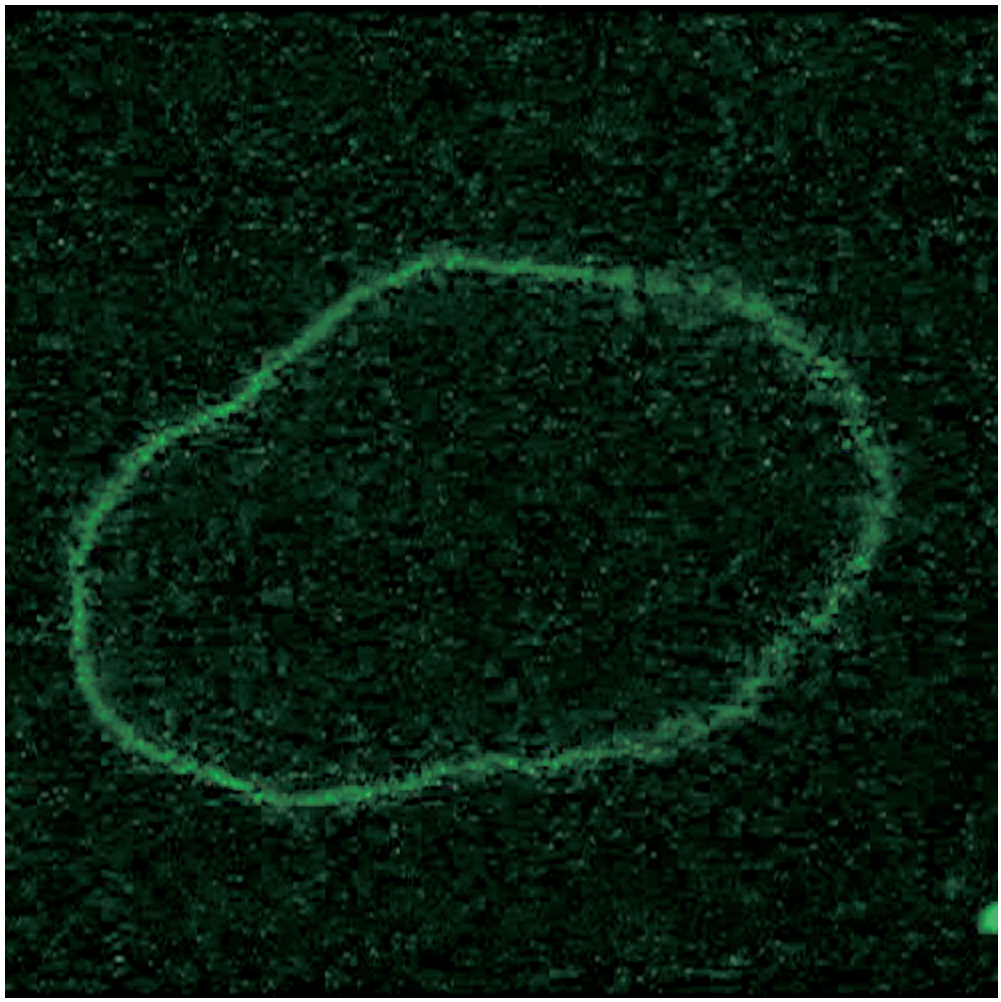

Movie S8. Streptolysin-O (SLO) was used to strongly reduce membrane tension. This movie shows a vesicle in the presence of 10 μg/ml SLO. The vesicles were incubated in the presence of 0.5 μM Arf1-OG (in green), 0.1 mM GTP and 2 mM EDTA. Strong shape fluctuations are observed in the presence of SLO indicating that membrane tension is very low. Even at low membrane tension, Arf1 alone does not induce budding or tubulation.

Movie S8 (MPG)

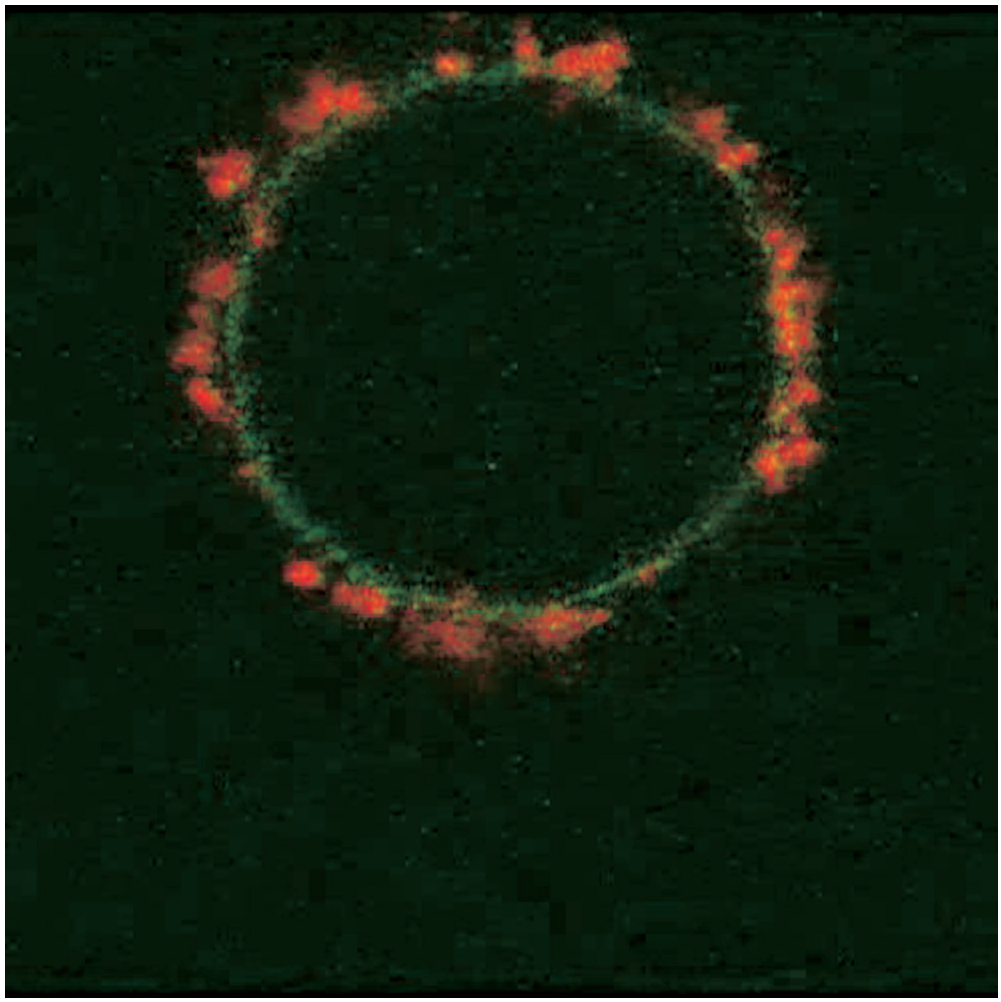

Movies S9. Dynamics of coatomer bound to a vesicle under very low membrane tension. Numerous deformation profiles covered with coatomer-TMR (in red) are observed on the surface of the vesicle (lipids are labeled by 0.5% C5-HPC-Bodipy-FL in green). Vesicles were incubated with 0.5 μM Arf1, 0.15 μM coatomer-TMR, and 10 μg/ml SLO in HKM buffer, 2 mM EDTA, and 0.1 mM GTP. $MgCl_2$ was then added to raise the Mg^{2+} concentration to 1 mM.

Movie S9 (MPG)

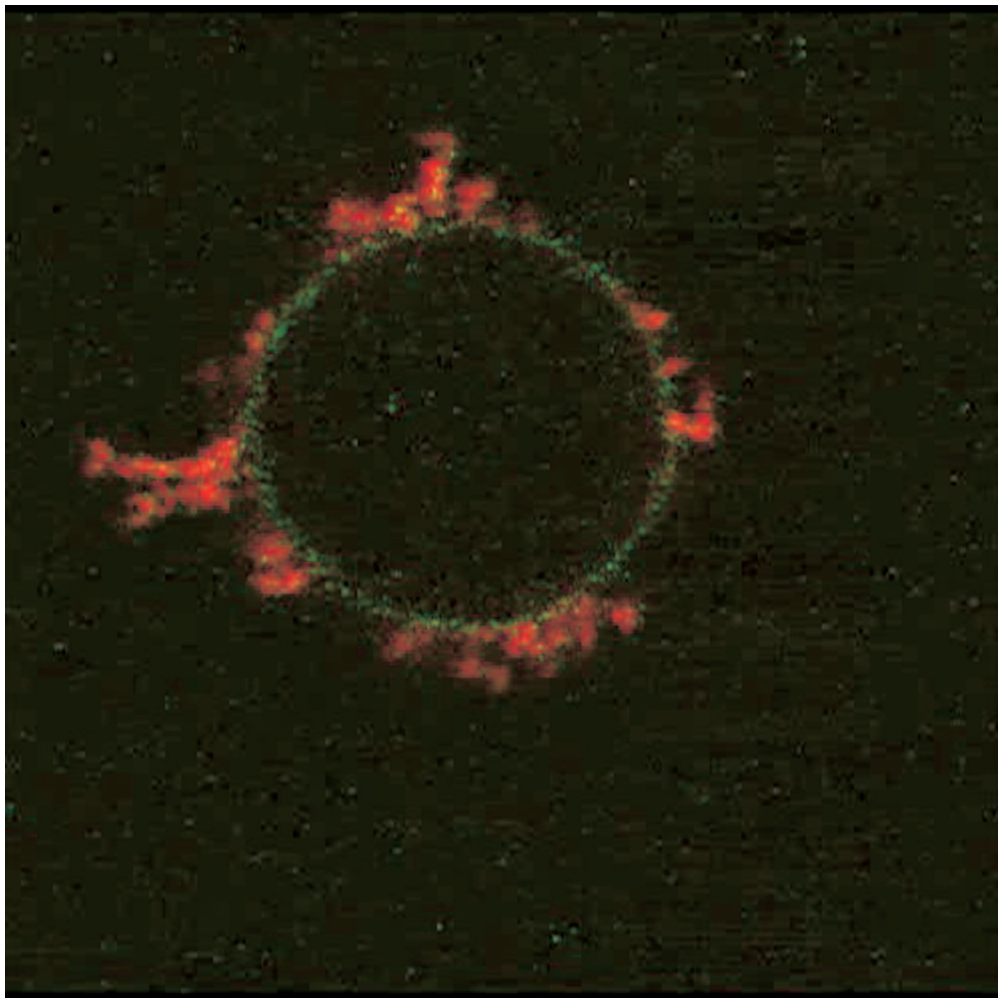

Movies S10. Dynamics of coatomer bound to a vesicle under very low membrane tension. Numerous deformation profiles covered with coatomer-TMR (in red) are observed on the surface of the vesicle (lipids are labeled by 0.5% C5-HPC-Bodipy-FL in green). Vesicles were incubated with 0.5 μM Arf1, 0.15 μM coatomer-TMR, and 10 μg/ml SLO in HKM buffer, 2 mM EDTA, and 0.1 mM GTP. $MgCl_2$ was then added to raise the Mg^{2+} concentration to 1 mM.

Movie S10 (MPG)

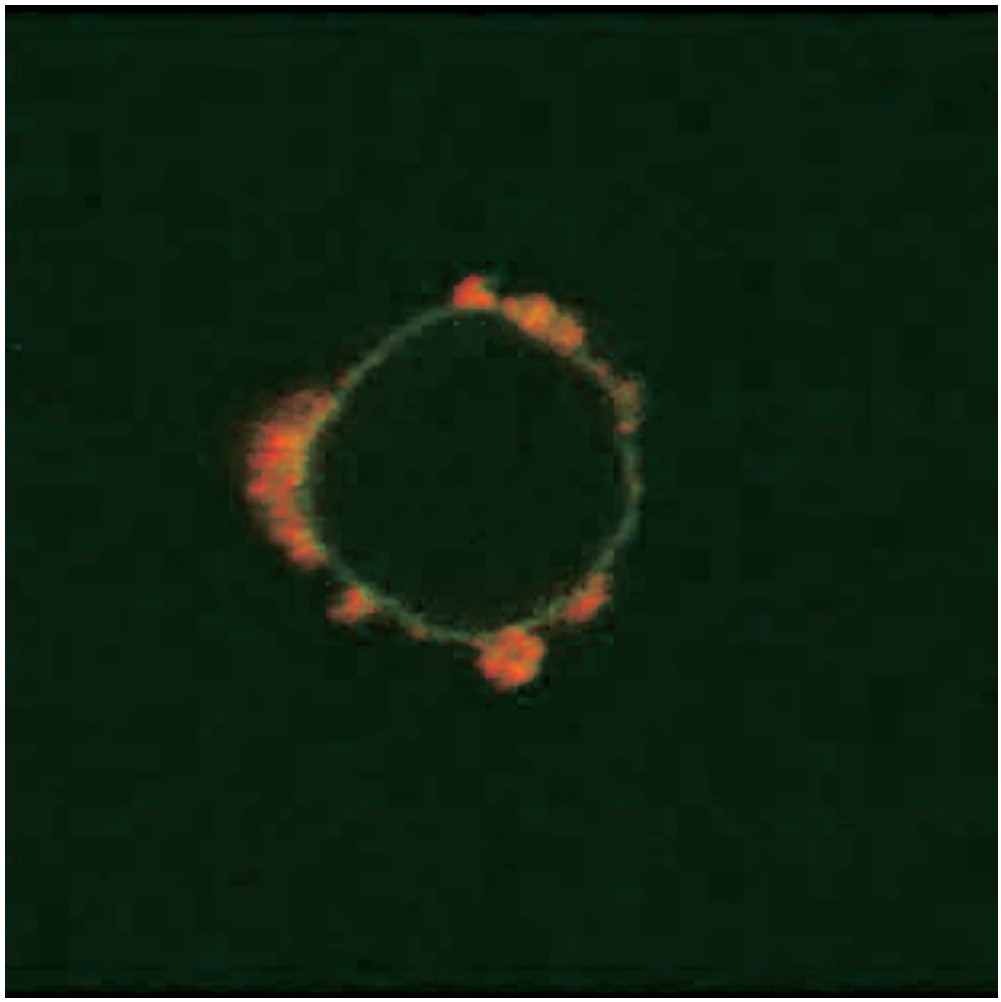

Movies S11. Dynamics of coatomer bound to a vesicle under very low membrane tension. Numerous deformation profiles covered with coatomer-TMR (in red) are observed on the surface of the vesicle (lipids are labeled by 0.5% C5-HPC-Bodipy-FL in green). Vesicles were incubated with 0.5 μM Arf1, 0.15 μM coatomer-TMR, and 10 μg/ml SLO in HKM buffer, 2 mM EDTA, and 0.1 mM GTP. $MgCl_2$ was then added to raise the Mg^{2+} concentration to 1 mM.

Movie S11 (MPG)

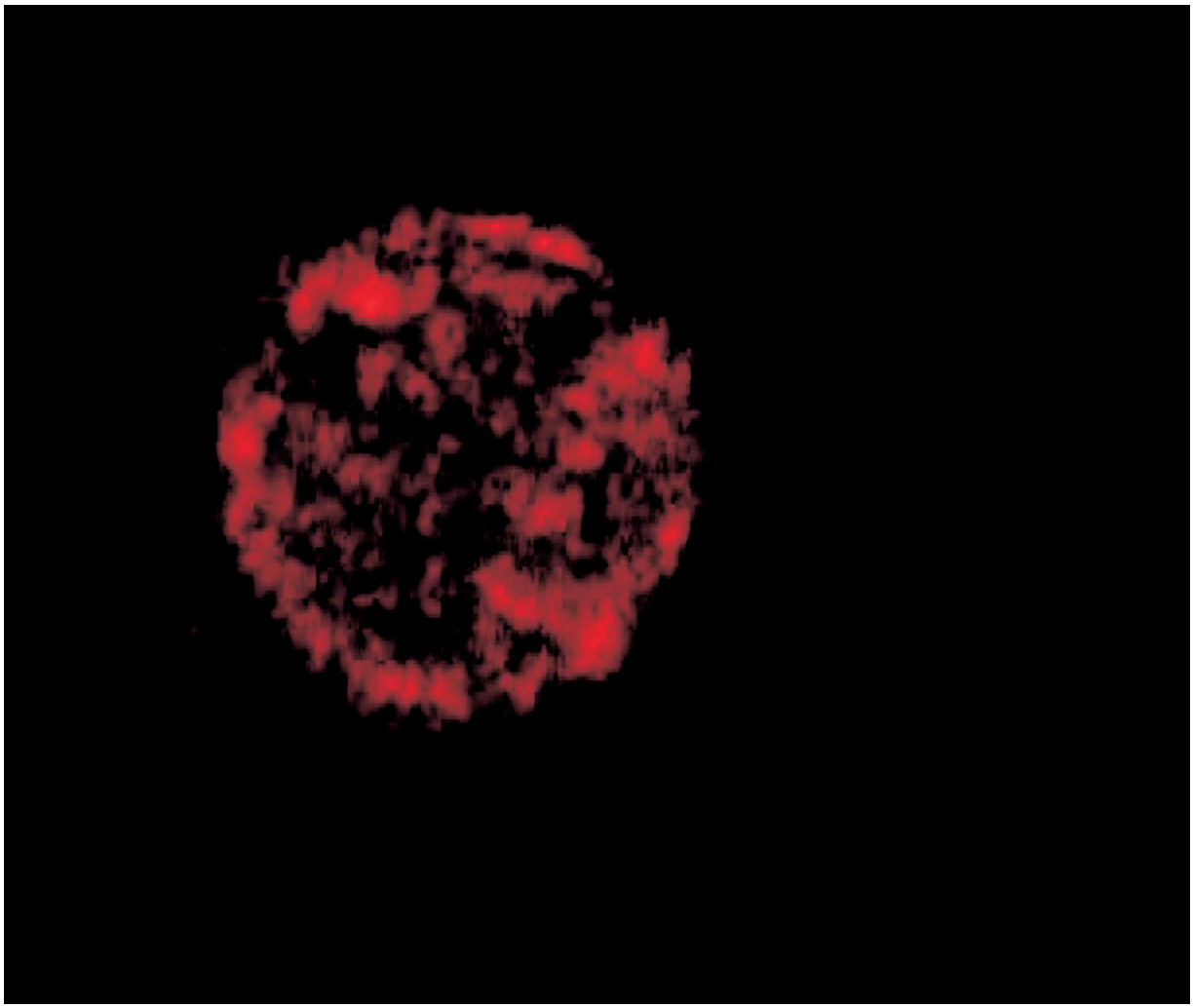

Movie S12. 3D reconstitution of coatomer bound to a SLO-treated vesicle. Coatomer-TMR is shown in red.

Movie S12 (MPG)

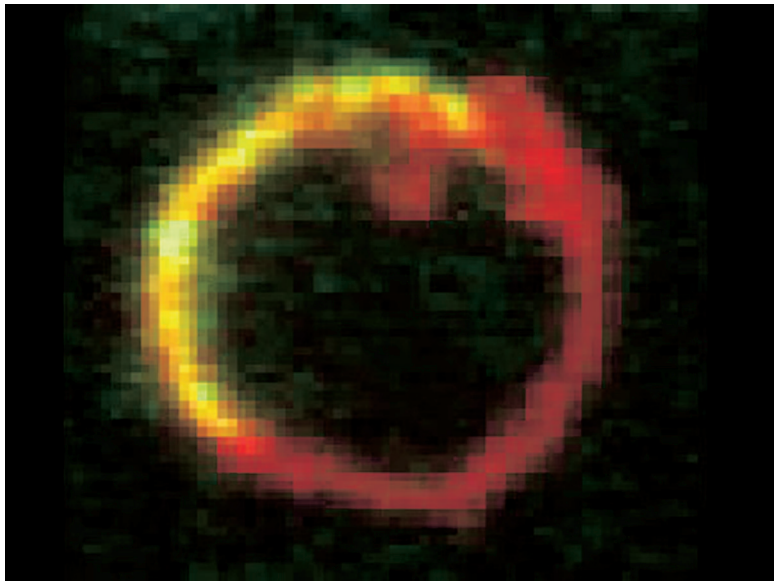

Movie S13. Reducing membrane tension after coat assembly does not modify the morphology of the coated membrane. Vesicles were first incubated with 0.5 μM Arf1, 0.15 μM coatomer, and fluorescently labeled anti-β-COP antibody (in green). SLO was then injected in the chamber at $\approx$10 μg/ml final concentration. Membrane fluctuations appeared only in the region of the vesicle that is not covered with coatomer. The membrane is labeled by 1% Ceramide-BodipyTR (shown in red). The yellow color shows the region where coatomer is bound to the membrane.

Movie S13 (MPG)

Table S1. Mobility of Arf1-OG

	Lipids	Arf	Arf + SLO
D, mm^2/s	6,38 ± 1,4	4,53 ± 0,33	4,81 ± 0,6
R, %	87,1 ± 2,2	92,7 ± 0,8	94,0 ± 1,1
N	26	38	36

The diffusion coefficient (*D*) and mobile fraction (*R*) of Arf1-OG were measured in the presence (Arf1 + SLO) or absence of SLO (Arf1) and compared to lipids (C5-HPC-BodipyFL). Arf1-OG diffusion in the GUV membrane is similar to lipids and does not depend on SLO. The average from *N* vesicles is given ± SEM.

Table S2.

	Lipids	Arf	coatomer
$t_{1/2}$, s	2.3 ± 0.3	2.7 ± 0.3	14.7 ± 2.2
R, %	67.7 ± 2.0	65.0 ± 1.4	30.6 ± 1.3
N	27	31	31

Mobility of coatomer-TMR compared to Arf1-OG and fluorescent lipids. The recovery time ($\tau_{1/2}$) and mobile fraction (*R*) of lipids, Arf1-OG and coatomer-TMR (in the presence of Arf1 and GTP) were measured from FRAP experiments (see *SI Materials and Methods*). Coatomer-TMR is much less mobile than Arf1-OG or fluorescent lipids, with a recovery about 5 times slower and a mobile fraction more than two times smaller. The maximum recovery is about 75% since typically a quarter of the GUV surface fluorescence is irreversibly bleached (see SI Materials and Methods). Recovery of coatomer-TMR is mostly due to diffusion of small-sized non-bleached patches from non-bleached regions into the bleached region. The average from *N* vesicles is given ± SEM. Values of the mobility of three different fluorescent lipids were pooled (DHPE-TexasRed, C5-HPC-BodipyFL and ceramide-BodipyTR).